J|A|C|S
ARTICLES

Published on Web 03/10/2010

Single-Pot Biofabrication of Zinc Sulfide Immuno-Quantum Dots

Weibin Zhou, Daniel T. Schwartz, and François Baneyx*

Department of Chemical Engineering, University of Washington, Box 351750, Seattle, Washington 98195

Received November 5, 2009; E-mail: baneyx@uw.edu

Abstract: Quantum dots (QDs) are a powerful alternative to organic dyes and fluorescent proteins for biological and biomedical applications. These semiconductor nanocrystals are traditionally synthesized above 200 °C in organic solvents using toxic and costly precursors, and further steps are required to conjugate them to a biological ligand. Here, we describe a simple, aqueous route for the one-pot synthesis of antibody-derivatized zinc sulfide (ZnS) immuno-QDs. In this strategy, easily expressed and purified fusion proteins perform the dual function of nanocrystal mineralizers through ZnS binding sequences identified by cell surface display and adaptors for immunoglobin G (IgG) conjugation through a tandem repeat of the B domain of *Staphylococcus aureus* protein A. Although ≈4.3 nm ZnS wurtzite cores could be biomineralized from either zinc chloride or zinc acetate precursors, only the latter salt gives rise to protein-coated QDs with long shelf life and narrow hydrodynamic diameters (8.8 ± 1.4 nm). The biofabricated QDs have a quantum yield of 2.5% and blue-green ensemble emission with contributions from the band-edge at 340 nm and from trap states at 460 and 665 nm that are influenced by the identity of the protein shell. Murine IgG_1 antibodies exhibit high affinity (K_d = 60 nM) for the protein shell, and stable immuno-QDs with a hydrodynamic diameter of 14.1 ± 1.3 nm are readily obtained by mixing biofabricated nanocrystals with human IgG.

Introduction

Semiconductor nanocrystals or quantum dots (QDs) are a class of inorganic fluorophores that are becoming increasingly important in biology and medicine due to their exceptional optical properties which include broad absorption spectra, large Stokes shifts, narrow emission peaks with size-dependent tunability, high photostability, resistance to photobleaching, and suitability for multiplex analysis.[1−6] Some of the most popular QDs for biological applications consist of a 2−10 nm diameter crystalline cadmium selenide (CdSe) or cadmium telluride (CdTe) core that is grown from organometallic precursors and whose size determines the emission wavelength (from 450 to 650 nm for CdSe and from 500 to 750 nm for CdTe). To remove surface defects that quench fluorescence, increase photoluminescence efficiency, and provide physical and optical stability, an insulator shell of wider band gap material, typically zinc sulfide (ZnS), is grown onto the core.[7,8] These steps are usually performed at ≈250−350 °C in organic solvents using fairly toxic and expensive compounds (see ref 9 and references within). QDs synthesized at high temperatures have no solubility in aqueous solvents and require functionalization with hydrophilic ligands through cap exchange or encapsulation to become water-soluble. For biological applications, they must be further derivatized with biomolecules such as nucleic acids, peptides, protein receptors, and antibodies. The wide range of chemistries developed for these purposes have advantages and drawbacks that were recently reviewed by Medintz and co-workers,[5] but they universally add to the time and expense of making practically useful hybrid nanostructures.

Biological processes offer a "green" alternative to synthetic chemistry for semiconductor nanocrystal fabrication. For example, several yeast species produce glutathione-like compounds called phytochelatins in response to heavy metal stress and accumulate CdS nanocrystals into their vacuoles when exposed to cadmium ions;[10,11] *Escherichia coli* grown to stationary phase[12] or overexpressing *Schyzosacchamoryces pombe* phy-

(1) Chan, W. C. W.; Nie, S. *Science* **1998**, *285*, 2016–2018.
(2) Clapp, A. R.; Goldman, E. R.; Mattoussi, H. *Nat. Protoc.* **2006**, *1*, 1258–1266.
(3) Gao, X.; Cui, Y.; Levenson, R. M.; Chung, L. W.; Nie, S. *Nat. Biotechnol.* **2004**, *22*, 969–976.
(4) Jamieson, T.; Bakhshi, R.; Petrova, D.; Pocock, R.; Imani, M.; Seifalian, A. M. *Biomaterials* **2007**, *28*, 4717–4732.
(5) Medintz, I. L.; Uyeda, H. T.; Goldman, E. R.; Mattoussi, H. *Nat. Mater.* **2005**, 435–446.
(6) Michalet, X.; Pinaud, F. F.; Bentolila, L. A.; Tsay, J. M.; Doose, S.; Li, J. J.; Sundaresan, G.; Wu, A. M.; Gambhir, S. S.; Weiss, S. *Science* **2005**, *307*, 538–544.
(7) Dabbousi, B. O.; Rodriguez-Viejo, J.; Mikulec, F. V.; Heine, J. R.; Mattoussi, H.; Ober, R.; Jensen, K. F.; Bawendi, M. G. *J. Phys. Chem. B* **1997**, *101*, 9463–9475.
(8) Hines, M. A.; Guyot-Sionnest, P. *J. Phys. Chem.* **1996**, *100*, 468–471.
(9) Biju, V.; Itoh, T.; Anas, A.; Sujith, A.; Ishikawa, M. *Anal. Bioanal. Chem.* **2008**, *391*, 2469–2495.
(10) Dameron, C. T.; Reese, R. N.; Mehra, R. K.; Kortan, A. R.; Carroll, P. J.; Steigerwald, M. L.; Brus, L. E.; Winge, D. R. *Nature* **1989**, *338*, 596–597.
(11) Dameron, C. T.; Smith, B. R.; Winge, D. R. *J. Biol. Chem.* **1989**, *264*, 17355–17360.
(12) Sweeney, R. Y.; Mao, C.; Gao, X.; Burt, J. L.; Belcher, A. M.; Georgiou, G.; Iverson, B. L. *Chem. Biol.* **2004**, *11*, 1553–1559.

tochelatin synthase[13] can mineralize luminescent CdS nanoparticles, and tobacco mosaic virus is capable of templating the growth of CdS and PbS nanowires.[14] In addition to whole organisms, several unmodified biomolecules such as nucleotides,[15] DNA,[16] RNA,[17] and polyhistidine extensions[18] have been shown to mediate the synthesis of semiconducting nanoparticles from aqueous solutions. However, QDs produced by these approaches often exhibit high polydispersity[15,17] and low quantum yields[13] and may be difficult to purify to homogeneity and/or require extra steps for conjugation to a targeting or detection signal (e.g., an antibody).[1,4]

Solid binding peptides (SBPs) displaying high affinity for inorganic materials can be readily isolated using cell surface and phage display technologies.[19,20] In addition to their technologically useful adhesive[21−26] and morphogenetic[27] properties, SBPs can function as material synthesizers by contributing Gibbs free energy of adsorption (ΔG_{ads}) to their cognate material, thereby promoting nucleation and growth of specific inorganic phases.[28−38] In many cases, SBPs remain functional when engineered within permissive locations of larger protein scaffolds, allowing for the combination of biomineralizing and host protein specific activities. For example, we have shown that a designer protein consisting of a cuprous oxide (Cu_2O) inserted within the framework of the DNA binding protein TraI was suitable for nonequilibrium mineralization of ≈2 nm Cu_2O core−protein shell nanoparticles that could be assembled onto a circular DNA guide.[29]

Here, we report the identification of ZnS binding peptides by cell surface display and the design of easy-to-purify designer proteins that mediate the aqueous synthesis of luminescent ZnS wurtzite nanocrystals while acting as adaptors for single-pot immunoglobin G (IgG) conjugation.

Experimental Section

Selection of ZnS Binding Peptides. The FliTrx cell surface display system (Invitrogen, Carlsbad, CA) was used to select disulfide-constrained dodecameric ZnS binding peptides through five rounds of biopanning on ≈7 mm chunks of ZnS (Sigma) as described.[39] Randomly selected colonies were subjected to sequencing using the BigDye Terminator sequencing kit (Applied Biosystems) using either 5′-ATTCACCTGACTGACGAC-3′ as a forward primer or 5′-CCCTGATATTCGTCAGCG-3′ as a reverse primer. Seven clones lacking internal cysteine residues but exhibiting diverse physicochemical properties (Table 1) were selected for further studies.

Table 1. Physicochemical Characteristics of Selected ZnS Binding Sequences

Name	Sequence[a]	M_r (Da)	pI	Hydropathy[b]
CT25	*CGP*AVRGRNAIILVP*GPC*	1278.56	12.00	+0.858
CT43	*CGP*AGDSSGVDSRSV*GPC*	1136.14	4.21	-0.442
CT50	*CGP*APWAEKRSWGHF*GPC*	1471.64	8.80	-1.108
CT52	*CGP*PKEGRRQNETQE*GPC*	1471.55	6.75	-3.050
CT54	*CGP*DYARQGLFDTSL*GPC*	1385.50	4.21	-0.500
CT66	*CGP*RCDRLAAGWRDV*GPC*	1442.60	9.51	-1.142
CT81	*CGP*KGRPGRAEEEC*GGPC*	1313.39	6.23	-2.325

[a] Amino acids are color-coded as follows: hydrophobic, gray; acidic, red; basic, cyan; hydroxyl side chain, dark green; amide side chain, light green. Invariant tripeptides flanking the dodecamers are italicized. [b] Average hydropathy (GRAVY) score: positive scores denote hydrophobic sequences, whereas negative scores denote hydrophilic sequences. The higher (respectively, lower) the score, the more hydrophobic (respectively, hydrophilic) the sequence is.[64]

DNA Manipulations. To construct *E. coli* thioredoxin 1 (TrxA) variants displaying zinc sulfide binding sequences, pFliTrx derivatives identified as above were recovered using the QIAprep Spin Miniprep kit (Qiagen) and digested with *Apa*LI and *Rsr*II, and the 220 bp DNA fragment was recovered following low melting point DNA electrophoresis. Plasmid pT-Trx,[40] which encodes the *trxA* gene under transcriptional control of the T7 promoter, was digested with the same enzymes. The purified backbone was next ligated with DNA fragments encoding zinc sulfide binders. The resulting series of plasmids was named pTrx-CTx, where x corresponds to the number of the zinc sulfide binding sequence defined in Table 1. Fusion proteins consisting of a tandem repeat of the B domain from *Staphylococcus aureus* protein A followed by native TrxA or its zinc sulfide binding derivatives were constructed as follows. DNA cassettes encoding BB sequences were PCR-amplified from plasmid pPrA2[41] using primers 5′-ATCGATCCGCATATGACAGCTG-3′ and 5′-TATCATGGCATATGGGCCTTTG-3′, which

(13) Kang, S. H.; Bozhilov, K. N.; Myung, N. V.; Mulchandani, A.; Chen, W. *Angew. Chem., Int. Ed.* **2008**, *47*, 5186–5189.
(14) Shenton, W.; Douglas, T.; Young, M.; Stubbs, G.; Mann, S. *Adv. Mater.* **1999**, *11*, 253–256.
(15) Hinds, S.; Bradford, J. T.; Levina, L.; Sukhovatkin, V.; Dooley, C. J.; Roy, M. D.; MacNeil, D. D.; Sargent, E. H.; Kelley, S. O. *J. Am. Chem. Soc.* **2006**, *128*, 64–65.
(16) Patel, A. A.; Wu, F.; Zhang, J. Z.; Torres-Martinez, C. L.; Mehra, R. K.; Yang, Y.; Risbud, S. H. *J. Phys. Chem. B* **2000**, *104*, 11598–11605.
(17) Ma, N.; Dooley, C.; Kelley, S. O. *J. Am. Chem. Soc.* **2006**, *128*, 12598–12599.
(18) Ayral, B. P.; Benson, D. E. *Bioconjugate Chem.* **2007**, *18*, 585–589.
(19) Baneyx, F.; Schwartz, D. T. *Curr. Opin. Biotechnol.* **2007**, *18*, 312–317.
(20) Kriplani, K.; Kay, B. K. *Curr. Opin. Biotechnol.* **2005**, *16*, 470–475.
(21) Brown, S. *Nano Lett.* **2001**, *1*, 391–394.
(22) Dai, H.; Thai, C. K.; Sarikaya, M.; Baneyx, F.; Schwartz, D. T. *Langmuir* **2004**, *20*, 3483–3486.
(23) Kacar, T.; Zin, M. T.; So, C.; Wilson, B.; Ma, H.; Gul-Karaguler, N.; Jen, A. K.; Sarikaya, M.; Tamerler, C. *Biotechnol. Bioeng.* **2009**, *103*, 696–705.
(24) Sengupta, A.; Thai, C. K.; Sastry, M. S. R.; Schwartz, D. T.; Davis, E. J.; Baneyx, F. *Langmuir* **2008**, *24*, 2000–2008.
(25) Wei, J. H.; Kacar, T.; Tamerler, C.; Sarikaya, M.; Ginger, D. S. *Small* **2009**, *5*, 689–693.
(26) Zin, M. T.; Leong, K.; Wong, N. Y.; Ma, H.; Sarikaya, M.; Jen, A. K. *Nanotechnology* **2009**, *20*, 15305.
(27) Grosh, C.; Schwartz, D. T.; Baneyx, F. *Cryst. Growth Des.* **2009**, *9*, 4401–4406.
(28) Ahmad, G.; Dickerson, M. B.; Church, B. C.; Cai, Y.; Jones, S. E.; Naik, R. R.; King, J. S.; Summers, C. J.; Kröger, N.; Sandhage, K. H. *Adv. Mater.* **2006**, *18*, 1759–1763.
(29) Dai, H.; Choe, W. S.; Thai, C. K.; Sarikaya, M.; Traxler, B. A.; Baneyx, F.; Schwartz, D. T. *J. Am. Chem. Soc.* **2005**, *127*, 15637–15643.
(30) Mao, C.; Flynn, C. E.; Hayhurst, A.; Sweeney, R.; Qi, J.; Georgiou, G.; Iverson, B.; Belcher, A. M. *Proc. Natl. Acad. Sci. U.S.A.* **2003**, *100*, 6946–6951.
(31) Mao, C.; Solis, D. J.; Reiss, B. D.; Kottmann, S. T.; Sweeney, R. Y.; Hayhurst, A.; Georgiou, G.; Iverson, B.; Belcher, A. M. *Science* **2004**, *303*, 213–217.
(32) Naik, R. R.; Brott, L. L.; Clarson, S. J.; Stone, M. O. *J. Nanosci. Nanotechnol.* **2002**, *2*, 95–100.
(33) Naik, R. R.; Stringer, S. J.; Agarwal, G.; Jones, S. E.; Stone, M. O. *Nat. Mater.* **2002**, *1*, 169–172.
(34) Nam, K. T.; Kim, D. W.; Yoo, P. J.; Chiang, C. Y.; Meethong, N.; Hammond, P. T.; Chiang, Y.-M.; Belcher, A. M. *Science* **2006**, *312*, 885–888.
(35) Slocik, J. M.; Naik, R. R. *Adv. Mater.* **2006**, *18*, 1988–1992.
(36) Slocik, J. M.; Stone, M. O.; Naik, R. R. *Small* **2005**, *1*, 1048–1052.
(37) Tang, R. K.; Darragh, M. R.; Orme, C.; Guan, X. Y.; Hoyer, J. R.; Nancollas, G. H. *Angew. Chem., Int. Ed.* **2005**, *44*, 3698–3702.
(38) Umetsu, M.; Mizuta, M.; Tsumoto, K.; Ohara, S.; Takami, S.; Watanabe, H.; Kumagai, I.; Adschiri, T. *Adv. Mater.* **2005**, *17*, 2571–2575.
(39) Thai, C. K.; Dai, H.; Sastry, M. S.; Sarikaya, M.; Schwartz, D. T.; Baneyx, F. *Biotechnol. Bioeng.* **2004**, *87*, 129–137.
(40) Yasukawa, T.; Kanei-Ishii, C.; Maekawa, T.; Fujimoto, J.; Yamamoto, T.; Ishii, S. *J. Biol. Chem.* **1995**, *270*, 25328–25331.
(41) Saito, A.; Honda, S.; Nishi, T.; Koike, M.; Okazaki, K.; Itoh, S.; Sato, M. *Protein Eng.* **1989**, *2*, 481–487.

introduce *Nde*I sites at both 5′ and 3′ ends. Plasmid pTrx-CT43 was linearized with *Nde*I, dephosphorylated with shrimp alkaline phosphatase, and ligated with the *Nde*I-digested BB cassette. The resulting plasmid was named pBB-Trx-CT43. Other zinc sulfide binding derivatives were obtained by ligating *Rsr*II−*Apa*LI segments from the pTrx-CTx series into *Rsr*II- and *Apa*LI-digested pBB-Trx-CT43. The integrity of all constructs was verified by DNA sequencing.

Protein Purification. BL21(DE3) cells harboring pTrx-CTx or pBB-Trx-CTx plamids were grown overnight at 37 °C in 25 mL of LB medium supplemented with 34 μg/mL chloramphenicol. Seed cultures were used to inoculate 450 mL of the same medium, and cells were grown at 37 °C with shaking at 225 rpm to $A_{600} \approx 0.5$. Flasks were transferred to an orbital water bath held at 30 °C and shaken at this temperature for 10 min, and protein synthesis was induced with 1 mM of isopropylthiogalactopyranoside (IPTG). After 4 h, cells were collected by centrifugation at 3000*g* for 15 min and resuspended into 45 mL of buffer A (20 mM Tris-HCl, pH 7.5) containing 2.5 mM EDTA and 1 mM PMSF. Cells were disrupted by three cycles of homogenization on a French pressure cell operated at 10 000 psi, and the lysate was clarified by centrifugation at 14 000*g* for 15 min. Supernatants were heated for 10 min at 80 °C and aggregated proteins sedimented by centrifugation as above. The supernatants were diluted 4-fold with buffer A and loaded onto a 1 cm inner diameter chromatography column packed with 5 mL of DE52 cellulose (Whatman) and equilibrated in the same buffer. Contaminants were removed by washing the column at a flow rate of 2 mL/min with 20 mL of buffer A, followed by 20 mL of buffer A supplemented with 20 mM NaCl. Target proteins were eluted in buffer A supplemented with 100 mM NaCl. Fractions were pooled, desalted, and concentrated to ≈0.5 mg/mL using Amicon Ultra-15 centrifugal filter units with a 3 kDa cutoff membrane (Millipore). Purity was greater than 99% as determined by videodensitometric analysis of silver-stained gels.

Protein-Aided Quantum Dot Synthesis. Two different Zn salts (chloride and acetate) were used to test the ability of purified proteins to drive the mineralization of ZnS quantum dots. For experiments involving zinc chloride, proteins were combined with 500 μL of 2 mM $ZnCl_2$ and 20 mM Tris-HCl, pH 7.0 in a round-bottom 18 mm diameter culture tube, and the volume was adjusted to 2 mL with 20 mM Tris-HCl, pH 7.0. After 1 h incubation at room temperature, the tube was placed in a vortex mixer operated at high speed, and 500 μL of 2 mM Na_2S was added dropwise using an Eppendorf P20 Pipetman. The total concentrations of Zn^{2+} and S^{2-} were 0.4 mM and that of protein was 1 μM. A stirring bar was placed in the tube, and the solution was vigorously mixed for 5−10 min at room temperature. The tube was capped, and the mixture was transferred to a 37 °C incubator and aged for 1−7 days. Maximum photoluminescence was typically reached after 5 days. For experiments involving zinc acetate, 200 μL of a 5 mM stock solution of $Zn(CH_3COO)_2$ in ddH_2O was mixed in a round-bottom 18 mm diameter culture tube with 800 μL of 5 mM $NH_4(CH_3COO)$ in ddH_2O. The pH was adjusted to the desired value using 1 mM CH_3COOH or 10 mM NH_4OH (for experiments conducted at the optimal pH of 8.2, 250 μL of 10 mM NH_4OH was added to the mixture). Next, proteins were added, and the volume was adjusted to 2.3 mL using ddH_2O. The solution was held at room temperature for 1 h before dropwise addition of 200 μL of 5 mM Na_2S in ddH_2O, stirring, and aging, as above. The final concentrations of Zn^{2+} and S^{2-} were 0.4 mM and that of protein was 2 μM. Long-term sample storage was at 4 °C.

Analytical Techniques. Absorption spectra were measured on a Beckman Coulter DU640 spectrophotometer using 1 mL of sample. Photoluminescence (PL) emission spectra were recorded from 300 to 800 nm using 1 mL samples on a Hitachi F4500 fluorescence spectrophotometer with excitation at 280 nm and slit widths set at 2.5 nm spectral resolution. The wavelength region corresponding to the second-order diffraction peak of the excitation light was omitted. Photoluminescence excitation (PLE) spectra were collected at 350 nm (BB-TrxA::CT43) and 440 nm (BB-TrxA::CT43@ZnS) over the indicated range of excitation wavelengths on the same instrument. Hydrodynamic diameters were measured on a Malvern Zetasizer Nano-ZS dynamic light scattering instrument equipped with a 633 nm laser filter using 1 mL samples. Quantum yields (QY) were calculated using tryptophan in water for reference and the gradient method, as described.[42] Briefly, five dilute samples ($0.01 < A_{325} < 0.08$) of protein alone or protein-mineralized quantum dots in ddH_2O were excited at 325 nm to eliminate the contribution of the proteins' tryptophan fluorescence to emission, and integrated spectra were subtracted from one another. Similar measurements were conducted on dilute solutions of tryptophan in ddH_2O except that excitation was at 280 nm. The integrated fluorescence intensities were plotted against absorbance, and slopes were obtained from a least-squares regression analysis ($r > 0.99$). Nanocrystal quantum yields were obtained by multiplying the ratios of the slopes by the QY of tryptophan (14%). For transmission electron microscopy (TEM) analysis, samples (5 μL) were deposited on plasma-cleaned carbon-coated copper TEM grids and allowed to dry in air. Low- and high-resolution (HRTEM) TEM images, selected area electron diffraction (SAED) patterns with an aperture size of 40 μm, energy-dispersive X-ray (EDX) spectra, and high-angle annular dark field scanning transmission electron microscopy (HAADF-STEM) images were collected on a FEI Tecnai G2 F20 S/TEM operated at an accelerating voltage of 200 kV.

Native Agarose Electrophoresis. Samples of ZnS quantum dots prepared by BB-TrxA::CT43-induced mineralization using $Zn(CH_3COO)_2$ and a pH of 8.2 were concentrated 50 times by centrifugation at 4000g for 20 min on Amicon Ultra-4 centrifugal filter units with a molecular mass cutoff of 10 kDa (Millipore). For complex formation, a 20 μL aliquot of the concentrate was mixed with 30 μL of 5.0 mg/mL human IgG (Sigma) reconstituted in ddH_2O, corresponding to a ≈2-fold molar excess of BB-TrxA::CT43 over IgG oligomers. The solution was incubated at 4 °C for 2 h and mixed with 50 μL of sample buffer (20% glycerol, 0.2% bromophenol blue, 0.12 M Tris base). A 20 μL aliquot was loaded on 2% agarose gel made in 25 mM Tris-Cl, pH 8.5, 19.2 mM glycine.[43] An aliquot (4 μL) of the concentrated quantum dot solution corresponding to the same BB-TrxA::CT43 molarity (0.4 nmol), as well as samples of purified BB-TrxA::CT43, IgG, and a mixture of the two proteins at a 2:1 molar ratio, was loaded in adjacent lanes to serve as controls. The gel was submerged in 25 mM Tris-Cl, pH 8.5, 19.2 mM glycine, and electrophoresis was performed at a constant voltage of 50 V for 45 min at room temperature. Fluorescent bands were visualized by illumination at 302 nm on a UV table, and the gel was subsequently stained with 0.12% Coomassie brilliant blue R in 45% methanol and 10% acetic acid for 1 h and destained in 45% methanol and 10% acetic acid.

ELISA Assays. BB-TrxA::CT43-mineralized quantum dots prepared and concentrated as above were assayed for protein content using a Bradford assay. Dilutions ranging from 0.6 mg/mL to 1 ng/mL BB-TrxA::CT43 were made in coating buffer (0.293% $NaHCO_3$, 0.159% Na_2CO_3, pH 9.5), and samples (100 μL) were applied to the wells of a 96-well ELISA plate. Following overnight incubation at 4 °C, the wells were washed four times in PBS (10 mM KH_2PO_4, 137 mM NaCl, 2.7 mM KCl, pH 7.4) supplemented with 0.05% Tween-20. Wells were passivated by incubation with 200 μL of blocking buffer (0.1% BSA in PBS) for 1 h at room temperature. After four cycles of washing, 100 μL of a 2000-fold dilution of horseradish peroxidase (HRP)-conjugated antipenta-His mouse IgG_1 (Qiagen) was added. The plate was incubated for 1 h at room temperature and washed as above, and wells were supplied with 100 μL of substrate solution freshly prepared by dissolving 4 mg of *ortho*-phenylenediamine (OPD; Pierce #34005) in 10 mL of 100 mM phosphate citrate buffer, pH 5.0, supplemented with 5 μL of H_2O_2. After 20 min incubation at room temperature, the reaction

(42) Eaton, D. F. *Pure Appl. Chem.* **1988**, *60*, 1107–1114.
(43) Kim, R.; Yokota, H.; Kim, S. H. *Anal. Biochem.* **2000**, *282*, 147–149.

was quenched with 100 μL of 1 M H_2SO_4 and absorbance at 492 nm was measured on a VersaMax microplate reader (Molecular Devices).

Results and Discussion

Identification of ZnS Binding Peptides. We used the FliTrx cell surface display system[44] to identify disulfide-constrained dodecamers binding to zinc sulfide (ZnS) as described in the Experimental Section. In this system, random dodecapeptides are displayed as disulfide-constrained loops within the active site of *E. coli* thioredoxin 1 (TrxA), which is inserted within the major flagellar protein FliC. As is commonly observed when cell surface display is used to screen for solid binding peptides,[19,45,46] sequences obtained after biopanning did not converge toward a consensus (Supporting Information Table S1). However, 17 of 25 randomly examined clones contained both acidic (Arg, Lys, His) and basic (Asp, Glu) residues that were evenly distributed along the dodecamers and usually separated by hydrophobic (Ala, Val, Leu, Ile, Met, Phe, Tyr, Trp) and hydroxyl containing (Ser, Thr) amino acids. Among these clones, twin acidic residues were rare, but 8 paired basic residues (chiefly Arg-Arg and Lys-Lys) were present in the 17 peptides, a frequency lower than that observed in ZnO and Cu_2O binding dodecamers isolated by FliTrx display.[39] A second class of ZnS binders (8 out of 25) exhibited a more hydrophobic character that was associated with the presence of a stretch of up to 5 nonpolar residues. Interestingly, these sequences lacked acidic residues but retained at least one, and up to four basic amino acids. In both classes of binders, structural amino acids (Gly, Pro) punctuated the dodecamers, presumably to accommodate packing constraints and to allow for peptide presentation within a disulfide-bonded loop, which can play an important role in determining binding affinity and/or specificity.[47−49]

While an over-representation of charged residues was expected in view of the fact that electrostatic interactions are commonly implicated in stabilizing interactions between peptides and inorganic materials,[19] neither class of binders were significantly enriched in His, Met, and Ser (three residues that mediate ZnS binding as homohexamers)[50] or shared significant homology with a dominant, disulfide-constrained ZnS binding heptamer (*Cys*-Asn-Asn-Pro-Met-His-Gln-Asn-*Cys*) identified by phage display.[51] On the other hand, comparison with a set of linear dodecamers selected on ZnS via bacteriophage display[51] revealed that 3 of these peptides (Z6, Z8, Z11) shared the characteristics of our class I binders, while the others (Z10, Z15, Z35) could be categorized as class II (Supporting Information Table S1). These results are consistent with the emerging view that, while there are multiple solutions to the problem of inorganic binding, spacing and functionality of amino acids in an SBP determine material specificity.[19,50]

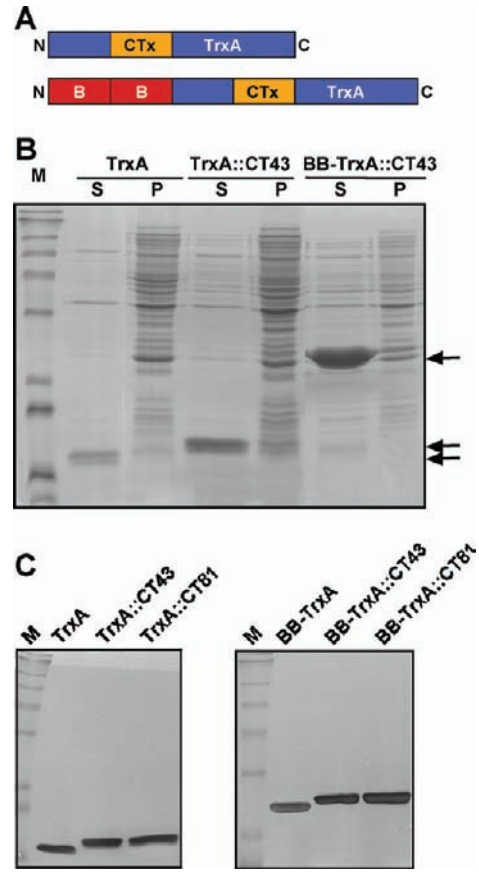

Figure 1. Expression and purification of ZnS synthesizing derivatives of TrxA. (A) Schematic structure of TrxA::CTx and BB-TrxA::CTx derivatives. Thioredoxin 1 (TrxA) protein framework is shown in blue, the zinc sulfide binding sequence in orange, and the tandem repeat of the B domain of staphylococcal protein A in red; amino and carboxyl termini are denoted by N and C, respectively. (B) Clarified extracts from cultures expressing authentic TrxA, TrxA::CT43, or BB-TrxA::CT43 were heated at 80 °C for 10 min and centrifuged at 14 000*g* for 15 min. Soluble (S) and insoluble pellet fractions (P) were analyzed by SDS-PAGE. (C) Silver-stained SDS minigels show that both TrxA and BB-TrxA derivatives are recovered with high purity following ion exchange chromatography.

Construction and Purification of Designer Proteins. To facilitate the identification of ZnS mineralizers, we transferred 7 sequences randomly selected on the basis of differences in pI and hydrophilicity (Table 1) into a plasmid encoding the *trxA* gene under transcriptional control of the T7 promoter. The resulting TrxA derivatives (TrxA::CTx, where x specifies the sequence number) are monomeric, range in molecular mass from 12.80 to 13.14 kDa, and contain the ZnS binding dodecamers flanked by invariant Cys-Gly-Pro and Gly-Pro-Cys tripeptides in place the Cys-Gly-Pro-Cys active-site sequence of wild-type TrxA. We further modified the TrxA::CTx series by fusing a tandem repeat of the 58 amino acids long B domain of *Staphylococcus aureus* protein A to their N-termini in order to endow them with the ability to bind the Fc fragment of IgG antibodies with high affinity[52−54] (Figure 1A). All

(44) Lu, Z.; Murray, K. S.; Van Cleave, V.; LaVallie, E. R.; Stahl, M. L.; McCoy, J. M. *Biotechnology* **1995**, *13*, 366–372.
(45) Sarikaya, M.; Tamerler, C.; Jen, A. K.; Schulten, K.; Baneyx, F. *Nat. Mater.* **2003**, *2*, 577–585.
(46) Sarikaya, M.; Tamerler, C.; Schwartz, D. T.; Baneyx, F. *Annu. Rev. Mater. Res.* **2004**, *34*, 373–408.
(47) Chen, H. B.; Su, X. D.; Neoh, K.-G.; Choe, W. S. *Langmuir* **2009**, *25*, 1588–1593.
(48) Choe, W. S.; Sastry, M. S. R.; Thai, C. K.; Dai, H.; Schwartz, D. T.; Baneyx, F. *Langmuir* **2007**, *23*, 11347–11350.
(49) Hnilova, M.; Oren, E. E.; Seker, U. O. S.; Wilson, B. R.; Collino, S.; Evans, J. S.; Tamerler, C.; Sarikaya, M. *Langmuir* **2008**, *24*, 12440–12445.
(50) Peelle, B. R.; Krauland, E. M.; Wittrup, K. D.; Belcher, A. M. *Langmuir* **2005**, *21*, 6929–6933.
(51) Flynn, C. E.; Mao, C.; Hayhurst, A.; Williams, J. L.; Georgiou, G.; Iverson, B.; Belcher, A. M. *J. Mater. Chem.* **2003**, *13*, 2414–2421.
(52) Jendeberg, L.; Nilsson, P.; Larsson, A.; Denker, P.; Uhlén, M.; Nilsson, B.; Nygren, P. Å. *J. Immunol. Methods* **1997**, *201*, 25–34.
(53) Jendeberg, L.; Perssoon, B.; Andersson, R.; Karlsson, R.; Uhlén, M.; Nilsson, B. *J. Mol. Recognit.* **1995**, *8*, 270–278.
(54) Langone, J. J. *Adv. Immunol.* **1982**, *32*, 157–252.

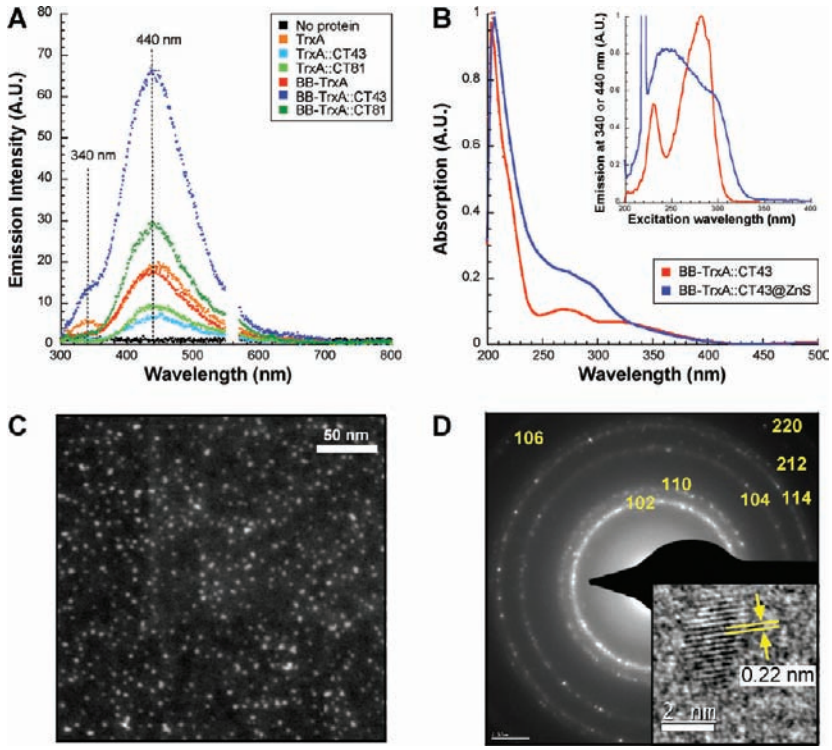

Figure 2. Characterization of ZnS nanocrystals biomineralized from a $ZnCl_2/Na_2S$ precursor electrolyte. (A) Emission spectra were collected for the indicated preparations following excitation at 280 nm. The spectral region corresponding to the second-order diffraction peak of the excitation light (560 nm) is omitted. (B) UV/visible absorption spectra of purified BB-TrxA::CT43 and of a QD solution mineralized by the same protein. The inset shows wavelength excitation scans on the same samples. HAADF-STEM (C), SAED (D), and HRTEM (inset) image of BB-TrxA::CT43-mineralized nanocrystals.

proteins were expressed with high yield and in a soluble form in *E. coli*.

Because TrxA exhibits high thermostability,[55] TrxA::CTx and BB-TrxA::CTx proteins could be purified to ≈70% homogeneity by heating crude cell extracts at 80 °C for 10 min and removing the insoluble material by centrifugation (Figure 1B). A subsequent ion exchange chromatography step led to the recovery of ≈99% pure material as judged by inspection of silver-stained SDS gels (Figure 1C). The presence of a disulfide bridge between cysteine residues flanking the CTx inserts was verified on selected proteins using AMS labeling as previously described[56] (data not shown).

Biomineralization of ZnS Quantum Dots from a $ZnCl_2$ Electrolyte. We initially tested the ability of the various TrxA derivatives (1 μM final concentration) to mediate the mineralization of optically active ZnS nanocrystals from a $ZnCl_2$ precursor electrolyte treated with Na_2S and aged for 5 days at 37 °C (see Experimental Section). In the absence of exogenously added protein, visible aggregates formed immediately after addition of Na_2S, and samples exhibited little photoluminescence upon excitation at 280 nm (Figure 2A, black).

Solutions prepared in the presence of TrxA derivatives were slightly turbid even when proteins were used at concentrations as high as 5 μM (data not shown), reflecting kinetic competition between protein-mediated stabilization of nanoscale colloidal particles and formation of bulk ZnS. Among the various proteins tested, TrxA::CT43 and TrxA::CT81 led to the appearance of a weak emission spectra with a single distinguishable peak centered at about 440 nm (Figure 2A, cyan and bright green). Interestingly, samples prepared in the presence of wild-type TrxA also exhibited photoluminescence. Spectral properties were comparable to those seen with TrxA::CT43 and TrxA::CT81, except for a ≈6 nm red shift in maximum emission and the appearance of a small peak at 340 nm (Figure 2A, orange). While we cannot exclude that the TrxA protein backbone contributes to the stabilization of ZnS nanocrystals, the most likely explanation for this result is that the highly reactive Cys32 residue of the TrxA active site, which is responsible for the formation of mixed disulfide with oxidized substrate proteins containing an incorrect disulfide bridge,[57] stabilizes ZnS nanocrystals by forming an adduct with surface Zn^{2+} atoms.

To our surprise, maximum emission intensities at 440 nm increased 10-fold when BB-TrxA::CT43 was substituted for TrxA::CT43 (Figure 2A, dark blue). However, the enhancement in emission intensity at λ_{Max} was only 3-fold when BB-TrxA::CT81 was used in place of TrxA::CT81, and there was little difference in the spectra of samples prepared in the presence of BB-TrxA or TrxA (Figure 2A). Considering that the three fusion proteins only differ by the presence and identity of a few amino acids in the TrxA active site, the large increase in emission observed with BB-TrxA::CT43 cannot be solely explained by folding or packing effects associated with the presence of the BB tandem repeat. Rather, the combination of a particular ZnS binding sequence and of the BB moiety is necessary to achieve enhanced luminescence through a mechanism that remains unclear but likely involves a combination of nanocrystal quality and modulation of surface effects that impact carrier relaxation and

(55) LaVallie, E. R.; DiBlasio, E. A.; Kovacic, S.; Grant, K. L.; Schendel, P. F.; McCoy, J. M. *Biotechnology* **1993**, *11*, 187–193.
(56) Schneider, E. L.; Thomas, J. G.; Bassuk, J. A.; Sage, E. H.; Baneyx, F. *Nat. Biotechnol.* **1997**, *15*, 581–585.
(57) Holmgren, A. *Annu. Rev. Biochem.* **1985**, *54*, 237–271.

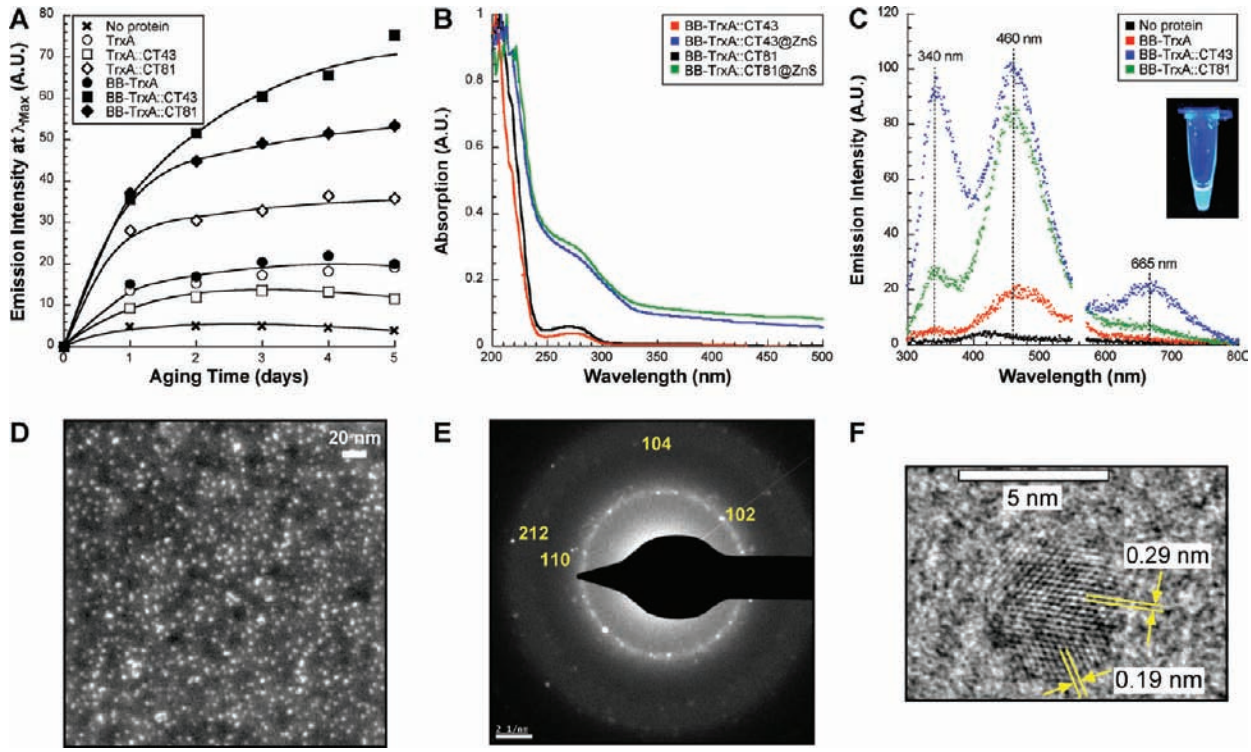

Figure 3. Characterization of ZnS nanocrystals biomineralized from a $Zn(CH_3COO)_2/Na_2S$ precursor electrolyte. (A) Evolution of maximum emission intensity for QDs mineralized with the indicated proteins over 5 days of incubation at 37 °C. Depending on the sample, maximum emission occurs at either 340 or 460 nm. (B) UV/visible absorption spectra of purified BB-TrxA::CT43 and BB-TrxA::CT81 (black) and of the nanocrystals mineralized by the same proteins. (C) Emission spectra of the indicated preparations were collected after excitation at 280 nm. The inset shows a concentrated solution of BB-TrxA::CT43-mineralized QDs exposed to UV light. HAADF-STEM (D), SAED (E), and HRTEM (F) images of nanocrystals obtained using BB-TrxA::CT43.

recombination processes.[58,59] Compared to a calculated emission band-edge of 317 nm for ZnS wurtzite and 340 nm for ZnS zinc blende, a major peak in the vicinity of 440 nm for all samples suggests that luminescence is primarily associated with surface (and possibly internal) trap states, with a small contribution from the band-edge in the case of TrxA and BB-TrxA::CT43. In all cases, the full width at half-maximum (FWHM) was ≈110 nm, which is significantly greater than that of the typical 30−50 nm FWHM value of QDs synthesized by traditional approaches, and likely reflects a broad density of states deep within the band gap.

We conducted a more detailed characterization of QDs mineralized by BB-TrxA::CT43. Figure 2B shows that the UV/vis absorption spectrum of the protein solution alone exhibits a maximum in the vicinity of 280 nm, which is consistent with the presence of 2 Trp and 2 Tyr residues, and that the absorption edge of the biomineralized nanocrystals (≈320 nm or 3.88 eV) is blue-shifted by 19 nm (0.22 eV) relative to bulk ZnS, as would be expected if the size of the nanoparticles was comparable to the Böhr exciton radius (≈2.5 nm). Similar results were obtained with other proteins (Supporting Information Figure S1A,B). To rule out the possibility that the QD emission peak at 440 nm upon irradiation at 280 nm results from fluorescence resonance energy transfer (FRET) between the Trp residues of BB-TrxA::CT43 and the nanocrystals, we recorded photoluminescence excitation spectra for both preparations (Figure 2B, inset). While BB-TrxA::CT43 alone exhibited the expected emission maximum at 340 nm when its aromatic residues were excited at 280 nm (red spectrum), there was no strong emission peak at 440 nm when the QD preparation was excited at the same wavelength (blue spectrum). Thus, photoluminescence is not associated with FRET phenomena. A quantum yield of 1.1% was determined using the gradient method and tryptophan as a standard (see Experimental Section).

Consistent with the requirements for quantum confinement, high-angle annular dark field scanning transmission electron microscopy (HAADF-STEM) images revealed that ZnS particles mineralized by BB-TrxA::CT43 were 4.2 ± 1.1 nm in size (Figure 2C), and their crystalline nature was confirmed by selected area electron diffraction (SAED) and high-resolution transmission electron microscopy (HRTEM) analysis (Figure 2D). Electron diffraction patterns of multiple particles could be uniquely indexed to the wurtzite (hexagonal) structure of ZnS (Figure 2D), a result confirmed by the 0.22 nm lattice spacing of selected nanocrystals (inset), which is only found in the wurtzite phase. Finally, dynamic light scattering (DLS) measurements performed on hydrated samples revealed the presence of a colloidal population at 10.5 ± 3.5 nm, a size expected for ZnS quantum dots surrounded by a 2−3 nm protein shell.

Unfortunately, although BB-TrxA::CT43@ZnS preparations could be stored for over a month at 4 °C with little loss in photoluminescence, centrifugation at 14 000*g* for 20 min or filtration of through a 0.2 μm membrane led to a 70−80% in emission, presumably reflecting entrapment of the QDs with large ZnS particles or aggregation.

Biomineralization of ZnS Quantum Dots from a Zinc Acetate Electrolyte. To address the above issue, we developed an alternative chemistry involving addition of Na_2S to a protein

(58) Jose, R.; Ishikawa, M.; Thavasi, V.; Baba, Y.; Ramakrishna, S. *J. Nanosci. Nanotechnol.* **2008**, *8*, 5615–5623.
(59) Wang, X.; Qu, L.; Zhang, J. Z.; Peng, X.; Xiao, M. *Nano Lett.* **2003**, *3*, 1103–1106.

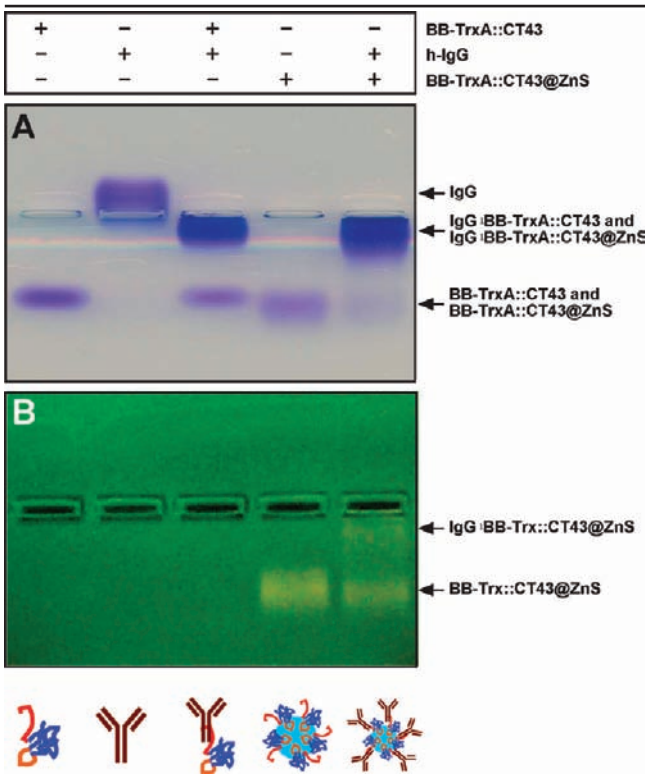

Figure 4. Efficient complex formation between human IgG and BB-TrxA::CT43-mineralized QDs. Soluble BB-TrxA::CT43, whole human serum IgG (h-IgG; mixed isotypes), and a complex obtained by mixing the fusion protein with the antibody at a 2:1 molar ratio were loaded on lanes 1−3. Samples of BB-TrxA::CT43-mineralized QDs alone and mixed with h-IgG at a 2:1 molar excess were loaded in lanes 4 and 5, respectively. The gel was stained with Coomassie blue (A) or photographed under UV light (B). The migration positions of the various proteins, binary complexes, and QD−protein complexes are identified by arrows and labeled. Cartoon representations are shown at the bottom.

containing $Zn(CH_3COO)_2$ solution (see Experimental Section). In agreement with the results of Figure 2, wild-type TrxA, TrxA::CT43, and TrxA::CT81 all gave rise to weak optical activity with peak luminescence reached after 2 days, and there was little difference in emission intensities when nanocrystals were mineralized with either TrxA or BB-TrxA (Figure 3A). Also consistent with our expectations, fusion of the BB domain to the N-terminus of TrxA::CT43 and TrxA::CT81 enhanced solution luminescence with maximum emission arising after 5 days. However, unlike $ZnCl_2$-derived nanocrystals, these QD preparations were stable for months at 4 °C with minimal (10−25%) decrease in emission intensity upon centrifugation or filtration after 70 days of storage.

Although absorption spectra were similar to those obtained with the $ZnCl_2$ precursor (Figure 3B and Supporting Information Figure S1), emission spectra for BB-TrxA::CT81, and especially BB-TrxA::CT43-mineralized nanocrystals, showed increased contribution from band-edge emission at 340 nm and a deep trap state peak at 665 nm that may be associated with the protein shell (Figure 3C). As a result, concentrated BB-TrxA::CT43@ZnS QDs appear blue-green to the eye upon UV illumination (Figure 3C, inset). The quantum yield was 2.5%, which is over twice that measured for nanocrystals mineralized with the same protein from a zinc chloride precursor. HAADF-TEM images of these preparations showed that the particles were roughly spherical and 4.3 ± 1.1 nm in size (Figure 3D). DLS measurements yielded a distribution of 8.8 ± 1.4 nm, which is narrower than that obtained with a $ZnCl_2$ precursor and consistent with a core−shell architecture. Finally, SAED patterns of multiple particles (Figure 3E) could be indexed to the wurtzite phase of ZnS, and HRTEM analysis of selected nanocrystals revealed a lattice spacing of 0.29 nm, which corresponds to the (101) plane of wurtzite ZnS (Figure 3F; assignment of the 0.19 nm spacing is more ambiguous since it corresponds to both the zinc blende (220) plane and wurtzite (110) plane). Similar results were obtained with BB-TrxA::CT81@ZnS.

In short, BB-TrxA::CT43 (or BB-TrxA::CT81)-mediated mineralization from a zinc acetate/sodium sulfide electrolyte yields optically stable and fairly narrowly distributed QDs consisting of a 4.3 nm ZnS wurtzite core surrounded by a ca. 2 nm protein shell with ensemble emission in the blue-green region of the spectrum.

One-Step Synthesis of Immuno-Quantum Dots. If the BB domain of the fusion protein is functional when tethered to a crystalline ZnS core through the CT43 loop, it should be possible to generate immuno-QDs by the simple expedient of adding IgG antibodies to a solution of biofabricated nanocrystals. To determine if this was the case, we took advantage of the fact that BB-TrxA::CT43 and human IgG antibodies (h-IgG) migrate at distinct locations when electrophoresed on agarose gels (Figure 4A, lanes 1 and 2). When a 2-fold excess of soluble BB-TrxA::CT43 was mixed with total h-IgG, a new band migrating at an intermediate position and corresponding to complex formation was detected (Figure 4A, lane 3). Thus, the BB domain of the fusion protein is properly folded and retains Fc binding capability. As expected from protein-coated nanocrystals, BB-TrxA::CT43-mineralized QDs migrated as a less focused band at the position of the soluble fusion protein (Figure 4A, lane 4), and the band was fluorescent when the gel was exposed to UV light (Figure 4B, lane 4). Addition of a 2-fold molar excess of the biofabricated QDs to h-IgG led to efficient immuno-QD formation as evidenced by the complete disappearance of the IgG band and the concomitant appearance of an intermediate fluorescent band corresponding to IgG-decorated nanocrystals (Figure 4, lanes 5). This new species accounted for ≈40% of the total fluorescence, suggesting that, within experimental uncertainty, nearly all BB domains on the nanocrystal surface are functional for IgG binding. Finally, DLS measurements of immuno-QDs prepared at a 1:1 molar ratio of h-IgG to BB-TrxA::CT43 revealed a single peak of hydrodynamic diameter 14.1 ± 1.3 nm. Considering that the diameter of the soluble h-IgG used in our experiments is 8.1 ± 0.7 nm, a 60% increase relative to the size of BB-TrxA::CT43@ZnS nanoparticles is consistent with an architecture in which the Fc fragment of the antibodies becomes buried in the fusion protein shell through interactions with the BB domain, and only $(Fab')_2$ domains add to the size of the complex.

To quantify the strength of interaction between BB-TrxA::CT43-capped QDs and IgG antibodies, we conducted an ELISA assay in which increasing amounts of biomineralized nanocrystals coated onto the wells of a microplate were detected using horseradish peroxidase (HRP)-conjugated mouse IgG_1 antibodies. The equilibrium dissociation constant extracted from the Langmuir isotherm shown in Figure 5 was 60 nM. Although this value is lower than the K_d of 1 nM reported for the interaction of BB fragments with human IgG,[53] it still denotes tight binding of antibodies to the protein shell, and the lower affinity is in part explained by steric hindrances associated with the presence of HRP and the fact

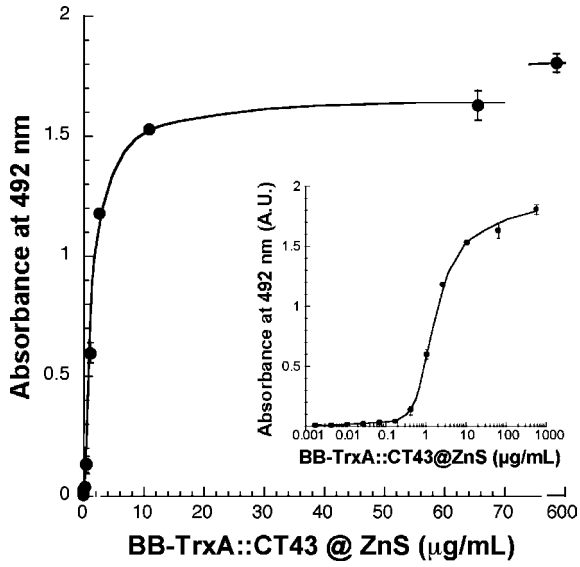

Figure 5. Mouse IgG_1 exhibits high affinity for BB-TrxA::CT43-mineralized QDs. Langmuir adsorption isotherm of horseradish peroxidase-conjugated mouse IgG_1 on BB-TrxA::CT43 shell ZnS core nanoparticles. The inset shows the same data on a semilogarithmic plot.

that staphylococcal protein A binds murine IgG less efficiently than human IgG.[52,60]

Conclusions

Traditional approaches for the production of immuno-QDs rely on the use toxic precursors, organic solvents and high temperatures for nanocrystal synthesis, and multiple derivatization steps to make QDs water-soluble and to conjugate them to antibodies.[61] Here, we have developed a simple route for the production of low-toxicity zinc sulfide immuno-QDs in which easily purified fusion proteins perform the dual function of nanocrystal mineralizer and adaptor for IgG conjugation. This molecular biomimetic[45,46] approach to functional nanostructure fabrication has the advantages of being performed in a few days under mild (37 °C) aqueous conditions and to allow "single-pot" synthesis of immuno-QDs with any IgG subtype(s) that interact strongly with staphylococcal protein A.[60]

Although ≈4 nm ZnS wurtzite nanocrystals could be mineralized by dropwise addition of sodium sulfide to a protein solution dispersed in either zinc chloride or zinc acetate, only the latter salt gave rise to protein-coated QDs exhibiting long shelf life and narrow hydrodynamic diameters (≈9 nm). For reasons that remain obscure, the presence of the BB domain significantly enhanced photoluminescence, which involves emission contributions from the band-edge at 340 nm and from trap states at 460 and 665 nm. At 2.5%, the quantum yield of BB-TrxA::CT43-mineralized ZnS QDs is lower than that of traditional CdSe/ZnS nanocrystals (typically 10−50%) but more than 350-fold higher than that reported for phytochelatin-mineralized CdS QDs.[13] Considering the simplicity of the synthesis method and its suitability for oriented display of unmodified antibodies, this is an acceptable trade-off. Although they do not emit in the tissue-transparent IR region of the spectrum, the ZnS-based immuno-QDs described herein are small (≈14 nm), should be significantly less toxic than their cadmium-based counterparts,[62] and biodegradable into innocuous components, three key requirements for clinical applications.[63] We are currently exploring the stability and usefulness of these structures for imaging and immunohistochemistry applications.

Acknowledgment. We are grateful to Corrine Thai for help with the selection of ZnS binding peptides, to Patrick Riley for assistance with protein purification, and to Xiaoxia Gao for assistance with TEM characterization. We thank David Ginger and Sam Jenekhe for helpful conversations, and Moriyuki Sato and Shunsuke Ishii for generous gifts of plasmids. This work was supported by the National Science Foundation (NSF) through a Protein-Aided Nanomanufacturing NIRT award (CMMI-0709131) and the Genetically Engineered Materials Science and Engineering Center (DMR-0520567). Part of this work was conducted at the University of Washington Nanotech User Facility, a member of the NSF National Nanotechnology Infrastructure Network.

Supporting Information Available: Complete table of ZnS binders and UV−vis absorption spectra of protein solutions alone and of nanocrystals biomineralized from zinc chloride and zinc acetate electrolytes. This material is available free of charge via the Internet at http://pubs.acs.org.

JA909406N

(60) Hober, S.; Nord, K.; Linhult, M. *J. Chromatogr. B* **2007**, *848*, 40–47.
(61) Xing, Y.; Chaudry, Q.; Shen, C.; Kong, K. Y.; Zhau, H. E.; Chung, L. W.; Petros, J. A.; O'Regan, R. M.; Yezhelyev, M. V.; Simons, J. W.; Wang, M. D.; Nie, S. *Nat. Protoc.* **2007**, *2*, 1152–1165.
(62) Rzigalinski, B. A.; Strobl, J. S. *Toxicol. Appl. Pharmacol.* **2009**, *238*, 280–288.
(63) Choi, H. S.; Liu, W.; Misra, P.; Tanaka, E.; Zimmer, J. P.; Ipe, B. I.; Bawendi, M. G.; Frangioni, J. V. *Nat. Biotechnol.* **2007**, *25*, 1165–1170.
(64) Kyte, J.; Doolittle, R. *J. Mol. Biol.* **1982**, *157*, 105–132.